Evaluations of prestack anisotropic Kirchhoff, Phase-shift-plus-interpolation and reverse-time depth migration methods for dipping TI media

Xiang Du, John C. Bancroft, Don C. Lawton and Laurence R Lines

ABSTRACT

Thick anisotropic sequences of dipping sandstones and shales often overlie the reservoir in fold and thrust belts, such as in the Canadian Foothills. In these cases, such an assumption, when anisotropy is negligible or only anisotropy with vertical symmetry axis (VTI) is considered, may result in imaging problems and mispositioning errors. Three prestack migration algorithms based on totally different principles, Kirchhoff, Phase-shift-plus-interpolation (PSPI), and reverse-time, are extended and presented for dipping TI media. Derived from the isotropic Kirchhoff, PSPI, and reverse-time migration methods, these three algorithms possess their own characteristics in accuracy and efficiency aspects. The ray-tracing algorithm used in 2-D prestack Kirchhoff depth migration is modified to calculate the traveltime in the presence of TI media with a tilted symmetry axis.

Based on an analytical solution of the quartic phase velocity equation for dipping TI media in the frequency-wavenumber domain, and an assumption for anisotropic parameters versus lateral velocities, the prestack anisotropic PSPI migration method can handle laterally variable anisotropic parameters and velocities. The prestack anisotropic reverse-time migration method employs the weak-anisotropy approximations to get the individual P-wave equation and implements depth migration with the pseudo-spectral method. Prestack anisotropic Kirchhoff depth migration still keeps its low cost isotropic algorithm advantage; however it suffers greatly from the difficulty of calculating the Green's function in media with both vertical and lateral variations in the space. Prestack anisotropic PSPI makes a good balance between computation efficiency and accuracy, but lacks the flexibility to deal with rapid spatial variation in the Thomsen parameters unless the reference wavefield is calculated for each pair of anisotropic parameters. The prestack anisotropic reverse-time method retains the isotropic algorithm's high cost character. The advantage of the method lies in the fact that it can handle arbitrary variable velocities and anisotropic parameters with excellent dipping angle imaging capability. Examples of migration on numerical and physical data with these three algorithms, shows imaging results can be improved by considering anisotropy parameters and the different characteristics of each method.

INTRODUCTION

Some hydrocarbon resource exploration and development projects are in areas containing dipping anisotropic sequences, such as in the Canadian Foothills (Isaac and Lawton, 1999). In these cases, depth migrations with either an isotropic migration algorithm or a vertical axis of symmetry (VTI) assumption will have imaging problems and positioning errors. Anisotropic depth migration is required to correctly locate images when dipping transversely isotropic (TI) strata are present. Many advanced migration

methods have been extended from isotropic to anisotropic media. Like isotropic methods, Anisotropic depth migration methods can be based on different equations and performed in different domains. These equations are related to the ray-tracing equation, the one-way wave equation, and the full wave equation. The domains include space-time, space-frequency, wavenumber-time, or wavenumber-frequency. The prestack anisotropic Kirchhoff migration method discussed in this paper is based on the ray-tracing equation and implemented in the $x-t$ domain. Prestack anisotropic PSPI starts from the one-way wave equation and carries on wavefield extrapolation in the $f-k$ domain. Prestack anisotropic reverse-time migration achieves recursive extrapolation backward in time with full wave equation in $x-t$ domain. Three representative methods are chosen to demonstrate the accuracy and efficiency characteristics of Kirchhoff, PSPI and reverse-time migration.

Kirchhoff migration is still the most popular migration in industry due to its low cost. There is no variation between isotropic and anisotropic Kirchhoff depth migration algorithm, only changing the traveltime tables in the presence of TI media. Tong et al. (1998) implemented Kirchhoff true amplitude migration technique for anisotropy media using a ray-tracing algorithm to compute the first-arrival traveltime and amplitude. Vestrum et al. (1999) similarly adopted a ray-tracing algorithm to obtain the traveltime to image structures below dipping TI media. Kumar et al. (2004) developed a direct method of traveltime computation in dipping TI media for use in Kirchhoff anisotropic depth migration. The traveltime calculations extended the Kirchhoff method further to be more accurate and moe easily applicable to seismic imaging.

In contrast to the Kirchhoff migration algorithm that is basically computationally unchanged in anisotropic media, the prestack anisotropic PSPI migration algorithm involves a more complicated phase-shift calculation. As a key to calculating the phase-shift terms in prestack anisotropic PSPI algorithm for dipping TI media, Le Rousseau (1997) used a table-driven interpolation method to get the approximation solution of vertical wavenumber k_x . Ferguson and Margrave (1999) presented an interpolation polynomial method to obtain the k_z approximately. Du et al. (2005) solved k_z analytically from the quartic dispersion equation. The PSPI depth migration method incorporates adaptation to lateral velocity variation through the wavefield interpolation. However with anisotropy parameters also varying along the lateral direction, it is important to identify the relationship between anisotropic parameters and velocities to reduce calculation for reference wavefields.

Reverse-time migration (McMechan, 1983; Wu et al., 1996; Yoon et al., 2003) is a very expensive method compared with the above two migration method. Reverse-time migration propagates the measured wavefield backward in time using a hyperbolic wave equation. The two-way hyperbolic wave equation does not suffer from dip limitation of the one-way downward continuation algorithms and handle multi-arrivals, steep dips, and overturned reflections. Du et al. (2005 a) computed solutions for the P- and SV-wave equations for the titled TI media and used them to implement a reverse-time migration. Although the algorithm is well adapted to the arbitrary variable velocities and parameters in spaces, it faces a new challenge in an increasing number of calculations.

In this paper, we will introduce the theory of three prestack anisotropic migration methods, and apply them to numerical and physical seismic data. In addition, we take into account the increase in calculation effort between each anisotropic migration algorithm and its isotropic case. In addition, we focus our work on the accuracy and efficiency comparison among the three anisotropic migration methods.

THEORY

Prestack anisotropic Kirchhoff depth migration method, prestack anisotropic PSPI method and prestack anisotropic reverse-time migration method will be introduced. We demonstrate the algorithm characteristics and illustrate the computational differences to the isotropic cases. We emphasize the core techniques of each algorithm.

Anisotropic Kirchhoff depth migration

As we mentioned above, the difference between the Kirchhoff anisotropic and isotropic migration algorithms lies in the traveltime calculation requiring no change in the Kirchhoff algorithm itself. A ray-tracing method (Kirtland Grech, 2002) is adopted to obtain traveltime tables for Kirchhoff depth migration. We start using the phase velocity equation (Tsvankin, 1996) written as

$$\frac{v^2(\theta)}{v_{p0}^2} = 1 + \varepsilon \sin^2\theta - \frac{f}{2} \pm \frac{f}{2}\sqrt{(1+\frac{2\varepsilon\sin^2\theta}{f})^2 - \frac{2(\varepsilon-\delta)\sin^2 2\theta}{f}}, \tag{1}$$

where v is phase velocity, as a function of phase angle θ, v_{p0} is vertical quasi-P wave velocity, v_{s0} is quasi-S wave velocity, $f = 1 - v_{s0}^2 / v_{p0}^2$ and ε and δ are Thomsen's parameters (Thomsen, 1986). Since we consider the depth migration algorithms for the P-wave, with linear weak anisotropy approximation, the phase velocity of the P wave is

$$v_p(\theta) = v_{p0}(1 + \delta\sin^2\theta\cos^2\theta + \varepsilon\sin^4\theta). \tag{2}$$

The corresponding derivative $dv_p(\theta)/d\theta$ is also computed as given in equation

$$\frac{dv_p(\theta)}{d\theta} = v_{p0}\{2\delta[\cos^3\theta\sin\theta - \cos\theta\sin^3\theta] + 4\varepsilon\cos\theta\sin^3\theta\}. \tag{3}$$

The relationship between the phase and group velocity is shown in equation

$$g = \sqrt{v_p^2 + \left(\frac{\partial v_p}{\partial\theta}\right)^2}, \tag{4}$$

and

$$\phi = \theta + \tan^{-1}(\frac{\partial v_p / \partial \theta}{v}), \tag{5}$$

where g is group velocity of P-wave, ϕ is the angle between the group velocity and symmetry axis and θ is the angle between the phase velocity and symmetry axis. Equation (4) gives the relationship between the magnitude of phase and group vectors. Equation (5) shows the relationship between the angles of the two vectors relative to the symmetry axis. For anisotropic ray-tracing, we ray trace across an interface with different anisotropy parameters according to Snell's law. Figure 1 illustrates the relationship among phase angle θ, ray angle ϕ, incident phase angle β, and incident ray angle α. At the same time, it can be found that

$$\alpha = \phi + \gamma, \text{ and } \beta = \theta + \gamma, \tag{6}$$

where γ is the angle of the TI symmetry axis. From the source position, a set of rays is emitted from a source location. When different rays arrive at an interface, the phase angles will be obtained by a scanning and interpolation with Equation (5) for a range of phase angle from 0^0 to 90^0. Since the ray parameter p is constant for a given ray across an interface, which is calculated from

$$p = \frac{\sin(\theta + \gamma)}{v(\theta)}, \tag{7}$$

we use the same method to get the refracted phase angle. In each layer, the Equation (4) is used to obtain the group velocity. Consequently the traveltime is generated from the ray path length over the group velocity. Through the traveltime interpolation, we get the traveltime table for each grid in the space.

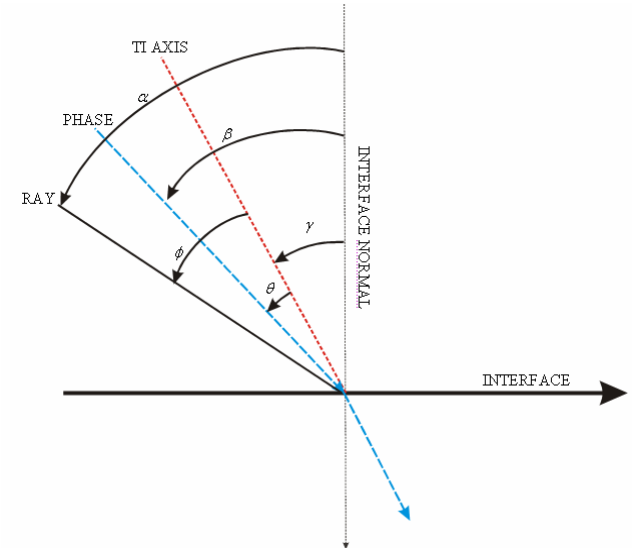

FIG. 1. The relationship between the ray and phase angles with the TI axis.

Anisotropic PSPI depth migration

Extending an isotropic PSPI algorithm to an anisotropic PSPI algorithm requires two key techniques. One is the vertical wavenumber calculation, and the other is the assumption of reference wavefields.

For the first problem, we start from the frequency-dispersion equation. Similarly to the isotropic case, we have the dispersion relationship in dipping TI media,

$$k_z = \pm\sqrt{\frac{\omega^2}{v^2(\theta,\phi)} - k_x^2}\ , \tag{8}$$

where ω is the frequency, $v(\theta)$ is the angle-dependent velocity, θ is the phase angle with the symmetry axis, and ϕ in the following parts denotes the tilt angle of the TI symmetry axis. In the isotropic case, ω and v are constant, so k_z can be readily computed from k_x , ω and v using the isotropic frequency dispersion equation. In anisotropic media, the angle-dependence of velocity makes the computation more complicated.

Using Equation (8) as the starting point, Le Rousseau (1997) precomputed a table of $k_z(\theta)$ and $k_x(\theta)$ while considering the angular dependence of velocity for anisotropic parameters. This requires locating or interpolating a given input k_x in the table, and finding the corresponding k_z . The accuracy of this table-driven algorithm is directly related to the size of the table; the finer the increment in phase angle θ, the better the result. With a larger table, the search time increases. Ferguson and Margrave (1998) suggested using an interpolating polynomial to get approximate solutions of k_z. They first estimated an empirical polynomial relationship between phase angle θ and horizontal slowness p by a series of numerical experiments, and then used the θ expression to calculation vertical slowness to get k_z. It seems that experiments are cumbersome with difference anisotropic parameters. A difficulty presents itself when the axis of symmetry ϕ of a TI medium is non-zero. The horizontal slowness versus phase angle for dipping TI medium shows that some values of p correspond to two values of θ, so we have to turn to other methods for a remedy. In fact, we can solve k_z analytically from the quartic dispersion equation. With Equation (1), when we rotate the symmetry axis from vertical to a titled angle ϕ, the phase velocity in the direction measured from the vertical direction is:

$$\begin{aligned}\frac{V^2(\theta,\phi)}{V_{p0}^2} &= 1+\varepsilon\sin^2(\theta-\phi)-\frac{f}{2} \\ &\pm\frac{f}{2}\sqrt{(1+\frac{2\varepsilon\sin^2(\theta-\phi)}{f})^2-\frac{2(\varepsilon-\delta)\sin^2 2(\theta-\phi)}{f}}\ .\end{aligned} \tag{9}$$

Substituting Equation (9) into Equation (8), we can get a quartic equation

$$k_z^4 + a_3 k_z^3 + a_2 k_z^2 + a_1 k_z^1 + a_0 = 0\,, \tag{10}$$

where a_i $(i = 0,1,2,3)$ is related to k_x, ε, δ, v_{p0} and ϕ. Two roots out of four of the quartic dispersion equation are chosen, one for down- and the other for upgoing-qP wave. Figure 2 shows a solution of the quartic dispersion equation for TI medium with a tilted angle of 30 degrees, $\varepsilon = 0.24$ and $\delta = 0.1$. The solutions solved by the Le Rousseau(1997) method are also shown in this figure with cyan color. The two solutions exactly match together.

As with the isotropic PSPI algorithm, several sets of reference parameters must be used for the migration. Ideally, reference wavefields would be generated for each set of reference parameters. Considering that we used four Thomsen parameters v_{p0}, ε, δ and ϕ, we would require 625 different sets of reference parameters. Han (2000) used the assumption that the anisotropy parameters are tied to reference values of the P-wave velocity. To make computation affordable, it is assumed that parameters v_{p0}, ε and δ have related lateral variation. Since tilted angle ϕ has a big effect on the wavefront dip direction, we take full account of the tilted angle.

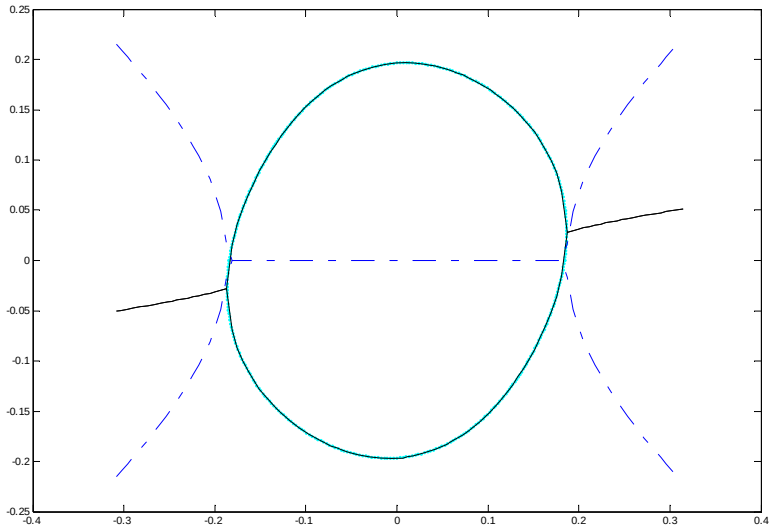

FIG. 2. Dispersion relationship of P-wave for a TI medium with 30^0 dipping angle The black solid lines denote the real part of *kz*, the blue dashed lines the are imaginary part of *kz* and the cyan solid lines represent the analytical solutions for the real part of *kz*.

Anisotropic reverse-time depth migration

It is straight forward to implement isotropic reverse-time migration with the acoustic equation. However, for anisotropic reverse-time migration, we get the appropriate P-wave equation first for dipping TI media. Du et al., (2005) discussed the individual P- and SV-wave equation for dipping TI media. Using Equation (1), with Thomsen approximation and the symmetrical axis rotated, the phase velocity of P-wave is

$$\frac{V_p^2(\theta,\phi)}{V_{p0}^2} = 1 + 2\delta \sin^2(\theta-\phi)\cos^2(\theta-\phi) + 2\varepsilon \sin^4(\theta-\phi) \tag{11}$$

For plane waves traveling in the vertical (x, z)-plane, the phase angle is given by

$$\sin\theta = \frac{v(\theta,\phi)k_x}{\omega}, \qquad \cos\theta = \frac{v(\theta,\phi)k_z}{\omega}. \tag{12}$$

Substituting equations (12) to Equation (11), multiplying it with the wavefields in the Fourier domain, and apply an inverse Fourier transform, we can obtain the P-wave equation for the tilted transverse isotropic media as

$$\begin{aligned}\frac{\partial^2 U_p(k_x,k_z,t)}{\partial t^2} = -V_{p0}^2[&k_x^2 + k_z^2 + (2\delta\sin^2\phi\cos^2\phi + 2\varepsilon\cos^4\phi)\frac{k_x^4}{k_x^2+k_z^2} \\ &+ (2\delta\sin^2\phi\cos^2\phi + 2\varepsilon\sin^4\phi)\frac{k_z^4}{k_x^2+k_z^2} \\ &+ (-\delta\sin^2 2\phi + 3\varepsilon\sin^2 2\phi + 2\delta\cos^2\phi)\frac{k_x^2k_z^2}{k_x^2+k_z^2} \\ &+ (\delta\sin 4\phi - 4\varepsilon\sin 2\phi\cos^2\phi)\frac{k_x^3k_z}{k_x^2+k_z^2} \\ &+ (-\delta\sin 4\phi - 4\varepsilon\sin 2\phi\sin^2\phi)\frac{k_z^3k_x}{k_x^2+k_z^2})]U_p(k_x,k_z,t)\end{aligned} \tag{13}$$

The implementation of prestack anisotropic reverse-time migration is same as the isotropic case. The procedure includes four parts:

(1) Determine the excitation-time imaging condition by anisotropic ray tracing to obtain traveltime from source position as we address the traveltime calculation for anisotropic Kirchhoff depth migration;

(2) Extrapolate the receiver wavefields backward in time using P-wave equation in anisotropic media shown in Figure 3;

(3) Apply the cross-correlated imaging condition;

(4) Sum the individual migrated shots to produce the final migration result.

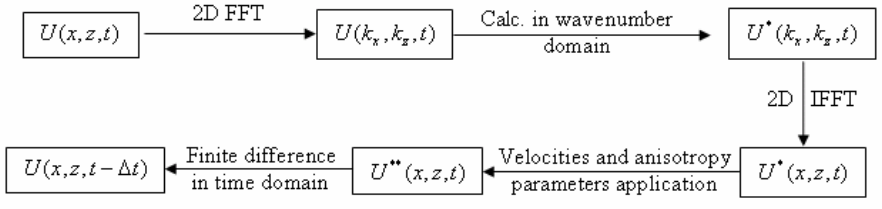

FIG. 3. The computation flow for implementing post-stack anisotropic reverse-time migration.

EXAMPLES

To evaluate the three anisotropic migration algorithms, two examples are chosen: one is numerically modeled data and the other is physically modeled data. Dip angles in each model illustrate the accuracy of angle imaging ability among three anisotropic depth migration methods.

Anisotropic imaging reflectors with different angles for variable velocity model

A variable velocity model is shown in Figure 4 that consists of six dipping reflectors (0, 15, 30, 45, 60, 75, 90 degrees). The medium has anisotropic parameters $\varepsilon = 0.2$, $\delta = 0.1$ and the tilt angle is 0. The velocity of the model is $v(x, z)$ =1500+0.3z +0.1x (m/s). The zero-offset synthetic data is shown in Figure 5. Figure 6 is the isotropic migration result obtained from isotropic PSPI migration method. The result is undermigrated without considering anisotropic situation. Correct imaging results using anisotropic Kirchhoff, anisotropic PSPI and anisotropic RT migration algorithms with exact anisotropic parameters, are shown in Figures 7, 8 and 9. The energy for the 90^0 reflector is weak for anisotropic Kirchhoff and APSPI migration results while the one for ART is better. The energy for reflectors with 75^0 and 60^0 by ART are stronger than that by anisotropic Kirchhoff and APSPI method. So we concluded that ART shows excellent ability in dip imaging. The anisotropic Kirchhoff method requires 1 minute, APSPI 5 minutes and ART 8 minutes for the computation. It seems that anisotropic Kirchhoff exhibits excellent computational efficiency, while APSPI makes a balance between the accuracy and efficiency. The overall comparison of computational cost is shown in Figure 10. It costs 1 minute, 4 minutes and 5 minutes for isotropic Kirchhoff, PSPI and RT. There isn't any cost increase between isotropic and anisotropic Kirchhoff migration methods since only the traveltime computation deals with anisotropic parameters. In addition, when we compare the computer run-time between isotropic and anisotropic cases for PSPI and reverse-time migration algorithms, because homogenous anisotropic parameters case is designated, the computation increment is relatively limited.

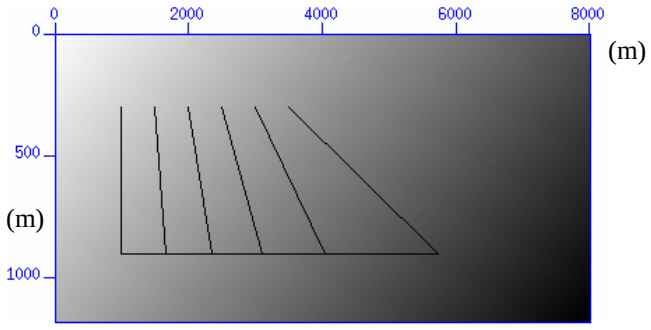

FIG. 4. A variable velocity model with homogenous anisotropic parameters that consits of six dipping reflectors.

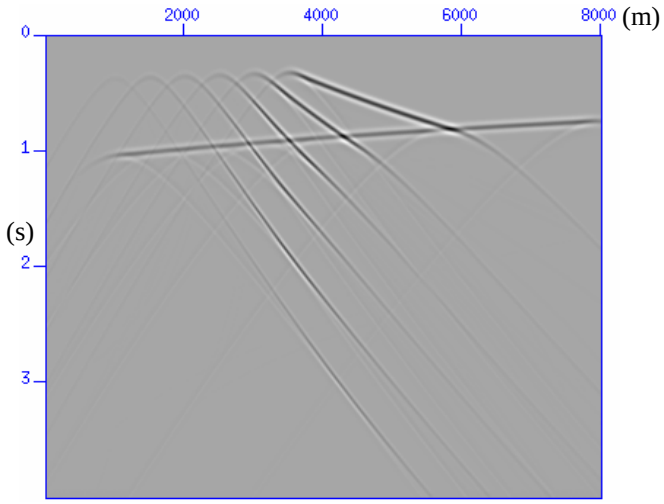

FIG. 5. The synthetic data for six dipping reflectors in the model of Figure 4.

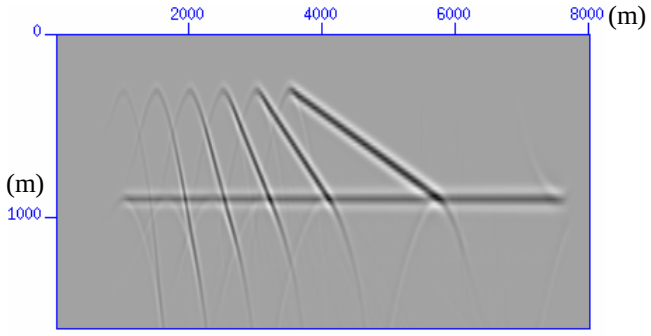

FIG. 6. Migration result by isotropic PSPI method.

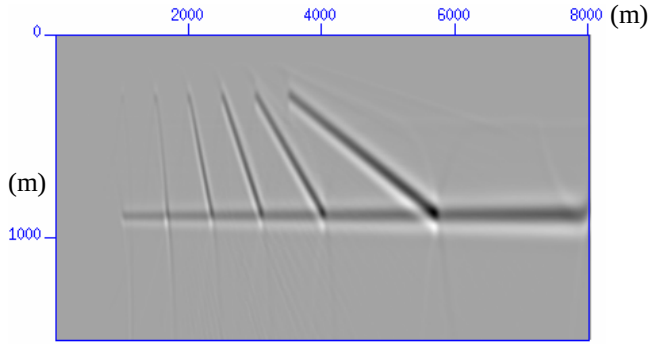

FIG. 7. Migration result by anisotropic Kirchhoff method.

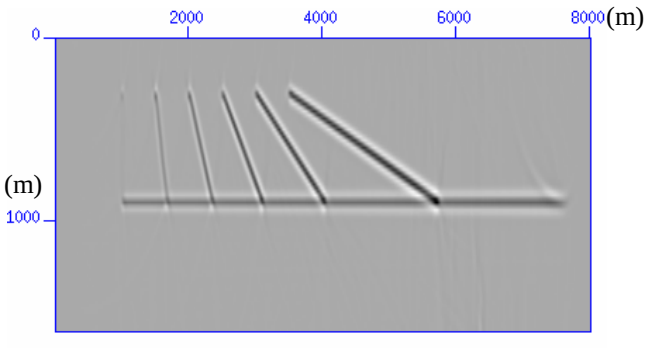

FIG. 8. Migration result by anisotropic PSPI method.

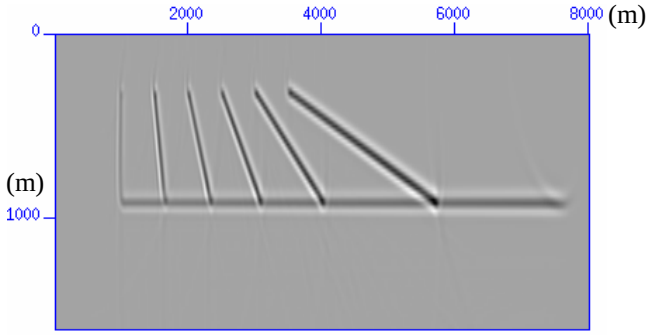

FIG. 9. Migration result by anisotropic reverse-time method.

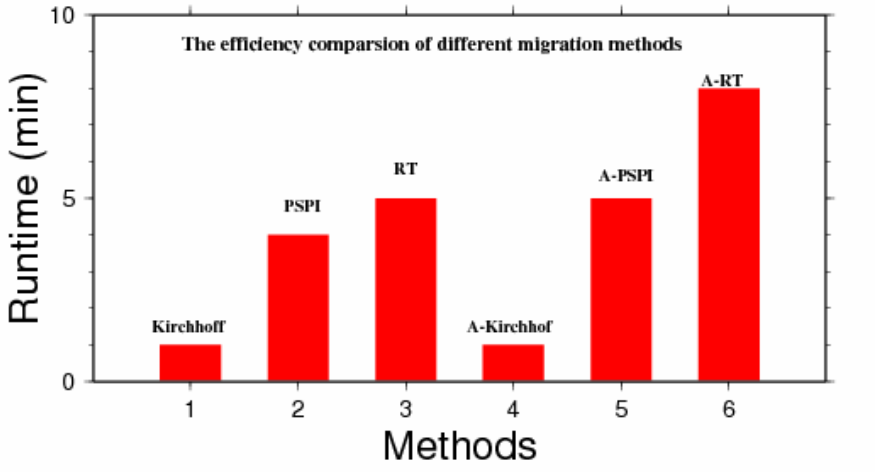

FIG. 10. The efficiency comparison between different methods.

Migration for TTI thrust sheet in an isotropic background

The physical model is a flat reflector overlain by a TI thrust sheet embedded in an isotropic background. The model is shown in Figure 11. The thrust sheet is composed of four blocks in the model; each with a unique axis of symmetry. They have parameters of $Vp0$ = 2925m/s, $\varepsilon = 0.224$ and $\delta = 0.100$. The isotropic background has a flat basement with $Vp0$ = 2740m/s. The prestack seismic dataset has 86 shot gathers acquired at 60m intervals along the line. Each source gather consists of 256 traces and 512 sample per

trace with 4ms sample rate. Figure 12 corresponds to the zero-offset seismic zone, where high velocity of the thrust structure overlying slow material causes the shadow zone between 2000m~3300m along the lateral direction. The shadow zone is the result of the zero-offset geometry in the recording. A normal incidence ray from the flat-lying reflectors beneath the thrust tends to strike the hanging wall at an angle greater than the critical angles, so that zero-offset reflections from the area beneath the steep thrust blocks are not possible for non-evanescent energy. Isotropic reverse-time migration produces a partially flat basement, however the basement beneath thrust sheets exhibits substantial pull up and the energy cannot be focused. Migration of the prestack data by anisotropic source-gather migration correctly positions the base reflector and fills the shadow zone due to the multiplicity of ray paths afforded by the prestack geometry.

Migration results for prestack anisotropic Kirchhoff, PSPI and RT migration (Figure 13, Figure 14, and Figure 15) show more accurate positioning of the reflectors and have nearly flattened the basement reflection, although the reflection event of the basement is not continuous. The migration result of prestack anisotropic reverse-time shows the stronger reflection energy for the dipping interfaces of the thrust structure. The imaging of the thrust structure is not as clear as we want since limited reference wavefields are applied. With respect to the computational efficiency, there is no increase (7 minutes)for prestack anisotropic Kirchhoff depth migration, as anisotropy only effects the traveltime calculation, which only amounts toa small part in the imaging process. However, due to a more complex physical model, the anisotropic wave equation algorithms greatly increase the computation effort. Isotropic PSPI uses 11 minutes whereas anisotropic PSPI takes almost 24 minutes. Similarly to the PSPI methods, isotropic reverse-time migration employs 15 minutes, but anisotropic reverse-time migration uses almost 60 minutes. The efficiency comparison is shown in Figure 17. Some noise exists in the APSPI migration result.

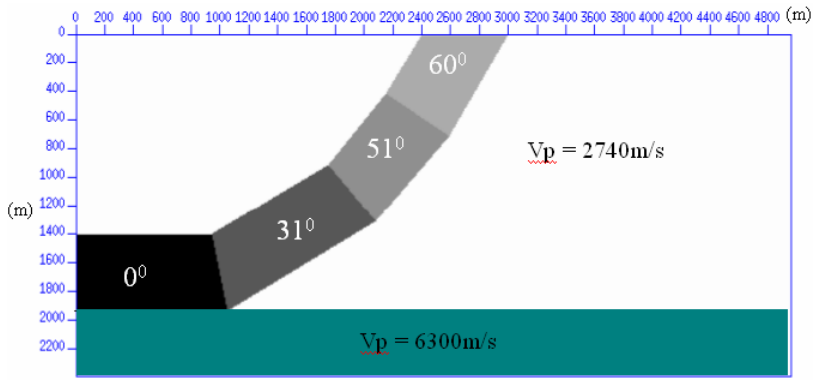

FIG. 11. Model of an anisotropic thrust sheet embedded in an isotropic background with same anisotropy parameters and different dipping angles.

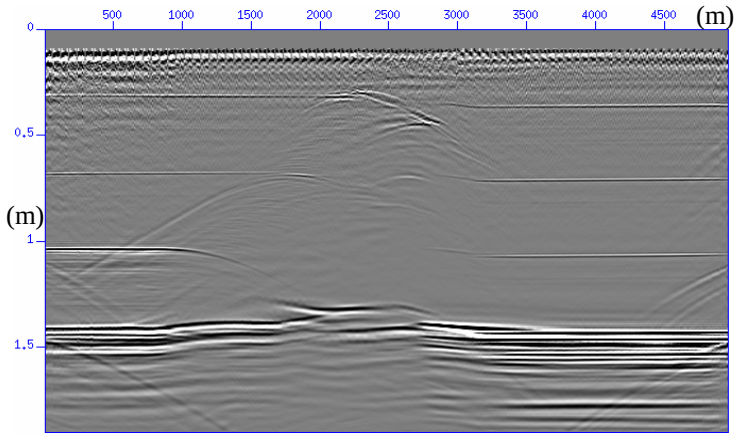

FIG. 12. The zero-offset seismic section sampled on thrust model.

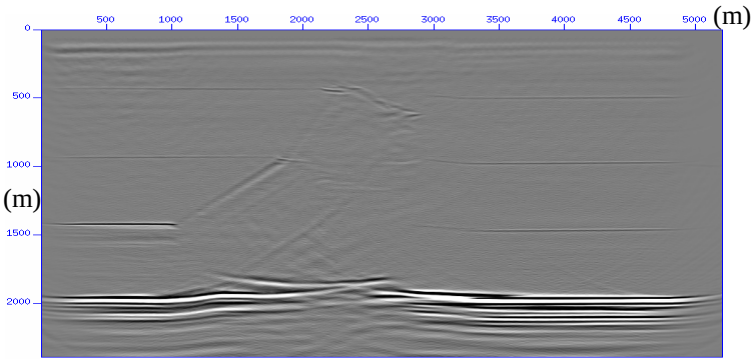

FIG. 13. Prestack migration result by isotropic reverse-time migration.

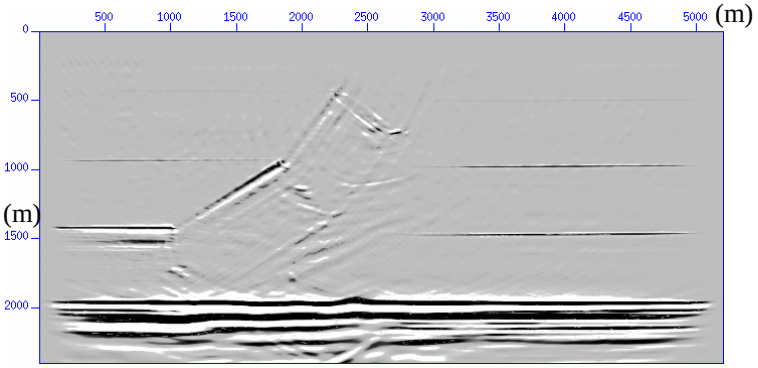

FIG. 14. Prestack anisotropic Kirchhoff depth migration result.

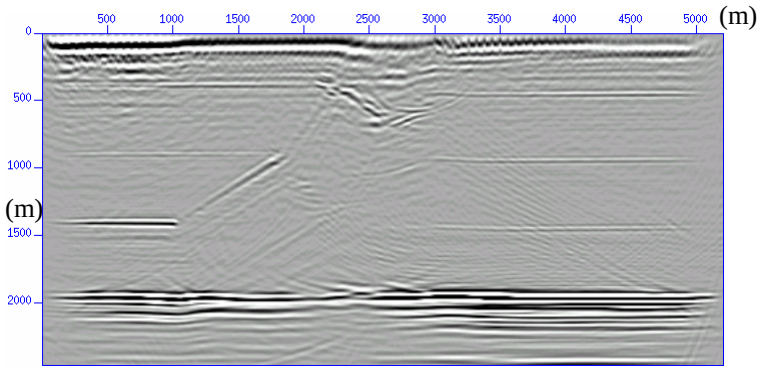

FIG. 15. Prestack anisotropic PSPI depth migration result.

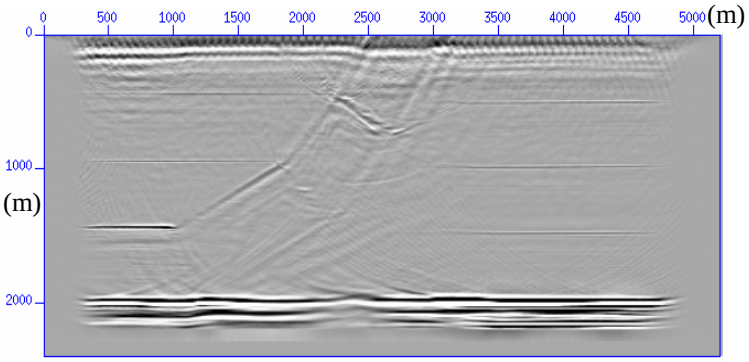

FIG. 16. Prestack anisotropic reverse-time depth migration result.

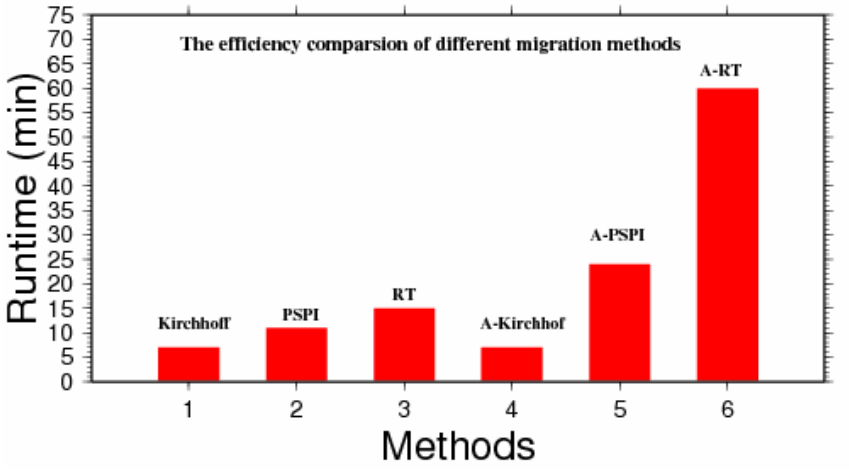

FIG. 17. Efficiency comparison among different isotropic and anisotropic migration algorithms.

CONCLUSIONS

From the above analysis, it is apparent that anisotropy has a large influence on the accuracy of migrated images. Use of a migration algorithm that takes anisotropy into account, with correct velocity information, can substantially improve images when anisotropy is present. In this paper, the traveltime calculation in TTI media is presented for prestack Kirchhoff depth migration. The Kirchhoff migration method still keeps the efficiency advantage even for complicated anisotropic media since the anisotropy doesn't affect the computation time of the migration algorithms itself. The theory for the anisotropic PSPI algorithm theory for TTI media is introduced and a new way to get an analytical solution for vertical wavenumber is presented. Prestack anisotropic reverse-time migration theory is also reviewed here, and we present appropriate P- and S-wave equations to use in place of the isotropic acoustic wave equation employed in isotropic reverse-time migration. The pseudo-spectral method is used to solve these equations implementing reverse-time migration.

Numerical and physical examples, give a practical comparison for the three algorithms, both isotropic and anisotropic, with respect to both accuracy and efficiency. We find prestack anisotropic Kirchhoff, PSPI and RT are both encouraging and promising. Anisotropic Kirchhoff migration retains the greatest advantage in computational costs. Anisotropic RT migration shows excellent capability in dip angle imaging, whereas anisotropic PSPI is a good balance between accuracy and efficiency. Anisotropic PSPI uses almost twice the computations as isotropic PSPI, while the computational cost of anisotropic RT is nearly five times as large as that of isotropic RT. However, with the rapid development of computer hardware, the two wave-propagation anisotropic depth migration algorithms will be widely used in seismic imaging.

ACKNOWLEDGEMENTS

The research was funded by the CREWES project and sponsors are thanked for their support. X.D. also appreciates SEG and CSEG for scholarships.

REFERENCES

Du, X., Bancroft J. C. and Lines L. R., 2005a, Reverse-time migration for tilted TI media: 75th Mtg. Soc. Expl. Geophys., Expanded Abstracts.

Du, X. Bancroft J. C. and Lines L. R., 2005b, A comparison of anisotropic phase-shift-plus-interpolation and reverse-time depth migration method for tilted TI media, CREWES Report 2005.

Ferguson, R. and Margrave G. F., 1998, Depth migration in TI media by non-stationary phase shift. 68th SEG meeting, New Orleans, U.S.A., Expanded Abstracts, 1831-1834.

Han, B. N., 2000, Two prestack converted-wave migration algorithms for vertical transverse isotropy: 70th Mtg. Soc. Expl. Geophys., Expanded Abstracts.

Isaac, J. H., and Lawton, D. C., 1999, Image mispositioning due to dipping TI media: A physical seismic study: Geophysics, **64**, 1230-1238.

Kirtland Grech, M. G., 2002 Depth imagining of fault-fold structures: Ph.D. thesis, University of Calgary

Kumar, D., Sen M. K., and Ferguson, R. J., 2004, Traveltime calculation and prestack depth migration in tilted transversely isotropic media: Geophysics, **69**, 37-44.

Le Rousseau, J. H., 1991, Phase shift–based migration for transverse isotropy: 61st Mtg. Soc. Expl. Geophys., Expanded Abstracts, 993-996.

McMechan, G. A., 1983, Migration by extrapolation of time-dependent boundary values: Geophys. Prosp., **31**, 413-420.

Thomsen, L., 1986, Weak elastic anisotropy: Geophysics, **51**, 1954–1966.

Tong F., Joe A. D., Gary E. M., Jeffrey L. H., and Samuel H. G., 1998, Anisotropic true-amplitude migration: SEG Expanded Abstracts **17**, 1677 - 1679 .

Tsvankin, I., 1996, P-wave signatures and notation for transversely isotropic media: An overview: Geophysics, **61**, 467-483.

Vestrum, R. W., Lawton, D. C. and Schmid, R., 1999, Imaging structures below dipping TI media: Geophysics, **64**, 1239-1246.

Wu, W., Lines, L. R., and Lu, H., 1996, Analysis of higher-order, finite-difference schemes in 3-D reverse-time migration: Geophysics, **61**, 845-856.

Yoon, K., Shin, C, Suh, S., Lines, L. R., and Hong S., 2003, 3D reverse-time migration using acoustic wave equation: An experience with the SEG/EAGE data set: The Leading Edge, **22**, 38-41.